
Counting Rate Characteristics and Image Distortion in Preclinical PET Imaging During Radiopharmaceutical Therapy

Emma Mellhammar¹, Magnus Dahlbom², Johan Axelsson³, and Sven-Erik Strand^{1,4}

¹Division of Oncology and Pathology, Department of Clinical Sciences–Lund, Lund University, Lund, Sweden; ²Department of Molecular and Medical Pharmacology, David Geffen School of Medicine, UCLA, Los Angeles, California; ³Department of Physics, LTH, Lund, Sweden; and ⁴Division of Oncology and Pathology, Department of Clinical Sciences–Lund, Lund University, Lund, Sweden

PET may provide important information on the response during radiopharmaceutical therapy (RPT). Emission of radiation from the RPT radionuclide may disturb coincidence detection and impair image resolution. In this study, we tested the feasibility of performing intratherapeutic PET on 3 preclinical PET systems. **Methods:** Using ²²Na point sources and phantoms filled with ¹⁸F, as well as a phantom filled with either ^{99m}Tc or ¹⁷⁷Lu, we evaluated the coincidence counting rate and spatial resolution when both a PET and a therapeutic radionuclide were in the PET system. Because ^{99m}Tc has a suitable half-life and is easy obtainable, we used it as a substitute for a generic therapeutic radionuclide. **Results:** High activities of ^{99m}Tc deteriorated the coincidence counting rate from the ¹⁸F-filled phantom and the ²²Na point source on all 3 systems. The counting rate could be corrected to a high degree on one of the systems by its dead-time correction. Spatial resolution was degraded at high ^{99m}Tc activities for all systems. On one of the systems, ¹⁷⁷Lu increased the coincidence counting rate and slightly affected the spatial resolution. The results for high ¹⁷⁷Lu activities were similar to those for ^{99m}Tc. **Conclusion:** Intratherapeutic imaging might be a feasible method of studying the response to RPT. However, some sensitive preclinical PET systems, unable to handle high counting rates, will have count losses and may also introduce image artifacts.

Key Words: PET; radionuclide therapy; dead time; pile up; image distortion

J Nucl Med 2016; 57:1964–1970
DOI: 10.2967/jnumed.116.175539

The use of radiopharmaceutical therapy (RPT) to treat cancer has advanced in the last decade as more effective targeting molecules have been introduced (1). Today, high activities of radionuclides or radionuclide-labeled molecules are used clinically to treat such conditions as thyroid cancer (2), lymphomas (3,4), and neuroendocrine tumors (5). Hopes of expanding the field have grown with the development of effective labeling methods for

antibodies, peptides, and Affibody molecules, among others, to therapeutic radionuclides (6–8). As these compounds are developed, better tools for in vivo measurement of the therapeutic response in tumor tissue are needed.

Intratherapeutic imaging, that is, PET performed during RPT, would be of interest for evaluating the effect of therapy early. In preclinical studies of therapeutic radiopharmaceuticals, the ability to collect longitudinal data throughout the treatment would reduce the need to sacrifice many animals. Intratherapeutic imaging could enhance our understanding of treatment response and offer biomarkers such as perfusion and hypoxia to complement the standard in vivo evaluation metric, tumor size.

Many of the radionuclides used for therapy emit not only the radiation desirable for treatment, such as α -particles, β -particles, low-energy conversion electrons, and Auger electrons, but also photons and x-rays. Some of these have energies high enough to penetrate the body of a patient or animal. This can be useful in biodistribution measurements and dosimetry calculations. To study not only therapeutic effects but also absorbed dose and dose rate, it would be desirable to use a therapeutic radiopharmaceutical and a diagnostic radiopharmaceutical simultaneously.

PET, a common method of molecular imaging, detects uptake of positron-emitting radiopharmaceuticals. One example is ¹⁸F-FDG, which detects glucose distribution and, along with dynamic imaging and pharmacokinetics, enables measurement of tumor blood perfusion and metabolism over time. In preclinical work, such studies could further our understanding of RPT. The complex effects of hypoxia on tumor therapy, which are likely to have big implications in the design of treatment protocols, can be evaluated with several PET radiopharmaceuticals, such as ¹⁸F-fluoromisonidazole (9). PET also provides tracers for angiogenesis (10), tumor cell proliferation, and apoptosis (11), among others.

When PET is applied for intratherapeutic imaging, there may be a risk that photons emitted from the therapeutic radiopharmaceutical will compromise the performance of the system. Secondary γ -emissions from the therapeutic radionuclide can severely affect the acquisition. High rates of photon fluence will perturb the detection of coincidences, because the detector will be busy handling single events without corresponding events in an opposing detector element (i.e., decreasing the detector lifetime).

The fast acquisition and processing of coincidence data in modern clinical and preclinical PET systems can sort out detected single events that do not originate from an annihilation event or that have been scattered and have lost energy. To allow detection

Received Mar. 14, 2016; revision accepted Jul. 5, 2016.
For correspondence or reprints contact: Emma Mellhammar, Division of Oncology and Pathology, Department of Clinical Sciences–Lund, Barngatan 2B, SE-221 85 Lund, Sweden.
E-mail: emma.mellhammar@med.lu.se
Published online Jul. 28, 2016.
COPYRIGHT © 2016 by the Society of Nuclear Medicine and Molecular Imaging, Inc.

of annihilation photons—even if they do not deposit their full energy in the detector—and to allow small-angle scattered annihilation photons to contribute to the counting rate, the energy window is set widely at somewhere between 100 and 700 keV.

All photons interacting in the detector will occupy a part of the time available for the system to process the event (“live period”). Therefore, all events, including those that do not originate from a positron annihilation, increase the total counting rate. At high counting rates, the number of detected coincidences can be compromised because of dead-time and pile-up effects. Depending on the dead-time characteristics of the system, events are lost during the interval when the system is occupied with processing a previous event. Pile-up can both add and subtract events from the final number of coincidences detected. Two photons may, if piled up, fall within the energy window and therefore add to the number of detected events. Similarly, photons detected inside the energy window may be pushed over the upper energy level if piled up with a photon of sufficient but lower energy. Therefore, pile-up both reduces the statistical quality of the image and can cause mispositioning of true coincidence events (12).

The influence of a therapeutic radiopharmaceutical on a PET acquisition will depend on the activity, the photon or x-ray yield (Bremsstrahlung can be neglected), and the energy of the emitted photons.

In this study, we investigated the impact of intratherapeutic imaging on the performance of 3 different preclinical PET systems—in particular, the effect on coincidence counting rate and spatial resolution when high activities of therapeutic radionuclides were in the field of view during the acquisition.

MATERIALS AND METHODS

PET Systems

Three different preclinical PET systems were evaluated for intratherapeutic imaging. For two of them, Inveon (Siemens Medical Solutions) and NanoPET/CT (Mediso), the detectors are assembled in a ring geometry, whereas for the third, Genisys4 (Sofie BioSciences),

4 detector blocks are set up as a box. The Inveon and Genisys4 were located at the University of California, Los Angeles (UCLA), and the NanoPET/CT was located at Lund University Bioimaging Center. The characteristics of these systems have been published elsewhere (13–16), and their main characteristics are summarized in Table 1.

The data for all systems were reconstructed into 5-min frames with the manufacturer-recommended algorithms: maximum-likelihood expectation maximization (60 iterations) for the Genisys4, ordered-subset expectation maximization (18 iterations, 16 subsets) for the Inveon, and 2-dimensional ordered-subsets expectation maximization (5 subsets, 6 iterations) for the NanoPET/CT.

The 3 PET systems differ in presentation of counting rate data and user availability. These are commercial systems designed to be user-friendly, and they perform the data analysis in the background, presenting only the relevant results to the user. On the Inveon and Genisys4, true, prompt, and random coincidences are retrievable from the files created during the data acquisition (header file and list-mode file). On the NanoPET/CT, the coincidence rate and singles rate for each detector module are recorded each second in the list-mode file and in an associated “events rates file.” The coincidence rate is assumed to be the prompt coincidences, that is, with the random prompts included.

Counting Rate Measurements

Three different high-counting-rate measurements were performed using decaying sources and phantoms as summarized in Table 2. To imitate a therapeutic radionuclide in the field of view of the PET system—emitting photons in the same energy range as for therapeutic ^{177}Lu — $^{99\text{m}}\text{Tc}$ was introduced as a surrogate.

Counting Rate Capability with ^{18}F Source (Study 1). Study 1 was of the counting rate capability of each PET system. An ^{18}F source was measured for several hours, throughout its decay.

Counting Rate Capability with ^{22}Na Source and $^{99\text{m}}\text{Tc}$ Background (Study 2A). Study 2A followed the decay of $^{99\text{m}}\text{Tc}$ in an in-house-made mouse phantom in which a point source of ^{22}Na was placed. The half-life of ^{22}Na (2.6 y) is long compared with $^{99\text{m}}\text{Tc}$ (6.02 h) and can be considered a constant activity; that is, the annihilation rate due to it will not change for the duration of the measurement. The changes in

TABLE 1
PET System Characteristics

| Characteristic | Inveon | NanoPET/CT | Genisys4 |
|---------------------------------------|----------------|------------------|---------------|
| Detector material | LSO | LYSO:Ce | BGO |
| Crystal dimensions (mm ³) | 1.5 × 1.5 × 10 | 1.12 × 1.12 × 13 | 1.8 × 1.8 × 7 |
| Axial field of view (mm) | 127 | 95 | 94 |
| Transaxial field of view (mm) | 100 | 123 | 45 |
| Energy window (keV) | 350–650 | 400–600 | 150–650 |
| Coincidence window (ns) | 3.4 | 5 | 20 |
| Sensitivity (%) | 6.7 | 7.7 | 14 |
| Image spatial resolution (mm) | 1.8 | 1 | 1.4 |
| Energy resolution (511 keV) (%) | 14.6 | 19 | 18.0 |
| Crystal decay time (ns) | 47 | 41 | 300 |
| Number of detectors | 64 | 12 | 4 |
| Number of crystals per detector | 400 | 1,200 | 3,159 |

BGO = bismuth germanate; LSO = lutetium oxyorthosilicate; LYSO = lutetium yttrium orthosilicate.

TABLE 2
Specific Activities and Phantoms Used

| Study | Phantom | Activity (MBq) | | |
|-------|-------------------------|---|---|--|
| | | Inveon | Genisys4 | NanoPET/CT |
| 1 | Sphere*/NEMA | 270 (¹⁸ F) | 11 (¹⁸ F) | 250 (¹⁸ F) |
| 2A | Point source and block† | 500 (^{99m} Tc), 0.074 (²² Na) | 170 (^{99m} Tc), 0.074 (²² Na) | 550 (^{99m} Tc), 0.43 (²² Na) |
| 2B | Sphere | — | — | 480 (^{99m} Tc) |
| 2C | Point source and block† | — | — | 82 (¹⁷⁷ Lu), 0.43 (²² Na) |
| 3 | Sphere‡/NEMA | 7.7 (¹⁸ F), 110 (^{99m} Tc) | 0.85 (¹⁸ F), 0.71 (^{99m} Tc) | 12 (¹⁸ F), 64 (^{99m} Tc) |

*0.5 mL.

†²²Na point source placed in center channel; silicon tube pulled through surrounding 4 channels.

‡1.0 mL for ^{99m}Tc and 0.5 mL for ¹⁸F.

coincidence counting rate were then due to the influence of the photon fluence rate and decay of ^{99m}Tc.

Random Coincidences from ^{99m}Tc Background on NanoPET/CT (Study 2B). Study 2B obtained a measurement of random coincidences generated on the NanoPET/CT by measuring a ^{99m}Tc-filled phantom alone. The true coincidence counting rate obtained in Study 2A was revealed by subtracting the coincidence counting rate in Study 2B.

Counting Rate Capability with ²²Na Source and ¹⁷⁷Lu Background (Study 2C). Study 2C was like Study 2A but with the ^{99m}Tc being replaced by ¹⁷⁷Lu, a therapeutic radionuclide used for RPT.

Counting Rate Capability with ¹⁸F Source and ^{99m}Tc Background (Study 3). Study 3 was of the changes in counting rate seen in Study 1 on each PET system due to a background emission of photons from ^{99m}Tc. An ¹⁸F source was measured for several hours, throughout its decay, with ^{99m}Tc alongside the ¹⁸F source.

Phantoms

Three types of phantoms were used: spheric hollow phantoms (Hollow Sphere Sets (6); Data Spectrum), a National Electrical Manufacturers Association (NEMA) NU 4-2008 mouse phantom (Data Spectrum), and an in-house-made mouse phantom. The spheric phantoms were 0.5 and 1.0 mL in volume. In the NEMA mouse phantom, the 2 fillable 0.7-mL chambers were used. The in-house

mouse phantom (Fig. 1) consisting of an epoxy resin block (T.L. Hart, Inc.) with silicon tubes 0.8 mm in inner diameter to be filled with activity (for Studies 2A–2C and 3). The block measured 90 × 30 × 20 mm and had 5 channels drilled at varying depths—at the surface and 0.25, 0.5, 0.75, and 1.0 cm from the surface—with the point source being placed in the center channel. For studies performed on the NanoPET/CT, the point source encapsulated in plastic was too large to fit inside the channels. It was therefore placed on top of the phantom. Use of the phantoms with the different combinations of radionuclides is described in Table 2.

Radioactivity

¹⁷⁷Lu was purchased from IDB Holland, ^{99m}Tc was obtained from a ⁹⁹Mo/^{99m}Tc generator, and ¹⁸F was produced at the Cyclotron Unit at Skåne University Hospital in Lund. For studies at UCLA, ^{99m}Tc was obtained from Triad Isotopes Inc., and ¹⁸F was obtained from the UCLA Biomedical Cyclotron Facility. The main characteristics of the radionuclides are summarized in Table 3.

Spatial Resolution and Image Quality

To study the effect of the reconstructed images on spatial resolution from Studies 2A and 2C, the full width at half maximum and full width at tenth maximum were calculated for a line profile over the ²²Na source. The volume resolution was calculated as the product of the full width at half maximum or full width at tenth maximum in the x, y, and z directions of the image data.

RESULTS

Counting Rate Capability with ¹⁸F Source

The coincidence counting rate performance of the 3 PET systems as revealed in the phantom studies is shown in Figure 2. For ¹⁸F activities of up to 1.6 MBq, the single and coincidence counting rates on the Genisys4 steadily increased, but for higher activities they quickly dropped off because of a paralyzingly high dead time. The NanoPET/CT and Inveon detectors accept higher activities and could handle higher counting rates before dead time led to paralysis. The Inveon reached its maximum coincidence counting rate at 185 MBq of ¹⁸F, and the NanoPET/CT reach its maximum counting rate at 54 MBq of ¹⁸F.

Counting Rate Capability with ²²Na Source and ^{99m}Tc Background

The initial high activity of ^{99m}Tc placed in the PET system together with the 74-kBq ²²Na point source affected the coincidence

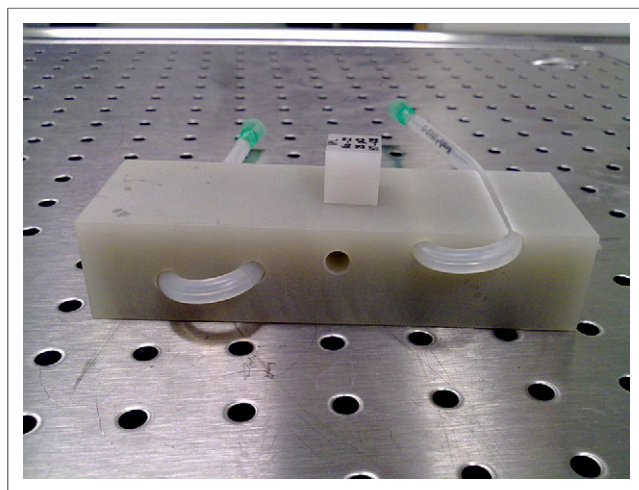


FIGURE 1. In-house-made mouse phantom with thin silicone tube drawn through the channels and point source placed on top.

TABLE 3
Radionuclides Used in This Report

| Isotope | Half-life | Decay mode | Q-value (keV) | Branching (%) | γ -emission (keV) | γ -yield (%) |
|--------------------------|-----------|--------------|------------------|---------------|--------------------------|---------------------|
| ^{177}Lu | 6.734 d | β^- | 498.3 | 100 | 113 208 | 6.4 11.0 |
| ^{18}F | 109.77 m | e, β^+ | 1,655.5 633.5 | 3.27 96.73 | — | — |
| $^{99\text{m}}\text{Tc}$ | 6.01 h | IT | — | 100 | 140.511 142.628 | 89 0.0187 |
| ^{22}Na | 2.6019 y | e, β^+ | 2,842.2 | 100 | 1,274.53 | 99.944 |

e = electron capture; IT = isomeric transition.

counting rate detected for all 3 systems (Figs. 3A–3C). The Genisys4 was continuously losing true coincidence counts with increasing activities of $^{99\text{m}}\text{Tc}$ during the interval examined (29–0.2 MBq). The number of random coincidences notably increased at between 1 and 8 MBq of $^{99\text{m}}\text{Tc}$. At even higher activities, all detected coincidences quickly decreased because of dead-time paralysis.

For the Inveon (Fig. 3B), the activity in the field of view during the initial time frame was 500 MBq of $^{99\text{m}}\text{Tc}$ together with the 74-kBq point source of ^{22}Na . Including the $^{99\text{m}}\text{Tc}$ reduced the detected true coincidence rate to about a third of that without $^{99\text{m}}\text{Tc}$ activity present. The number of coincidences was constant for activities of up to about 10 MBq. For activities of over 50 MBq, the number of detected coincidences fell approximately exponentially with increasing $^{99\text{m}}\text{Tc}$ activity. Random coincidences remained negligible for $^{99\text{m}}\text{Tc}$ activities of up to 250 MBq, at which point an increase was noticed. Correcting the true coincidence rate with the dead-time correction factor available on the Inveon compensated for the coincidence counting rate losses seen at $^{99\text{m}}\text{Tc}$ activities of over 50 MBq.

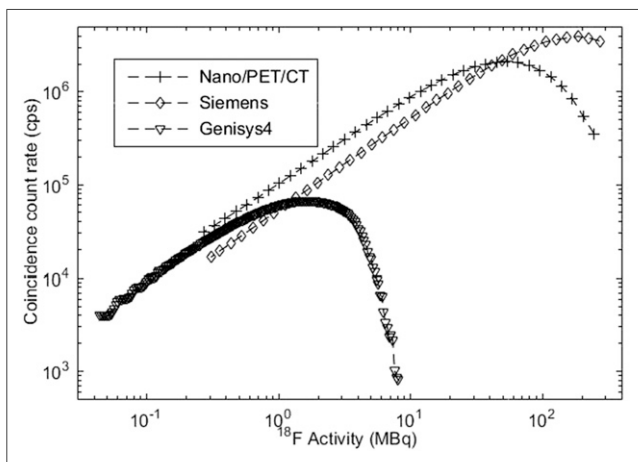


FIGURE 2. True coincidence counting rates detected on Genisys4, Inveon, and NanoPET/CT when high activities of ^{18}F were allowed to decay in PET system in Study 1. (On NanoPET/CT, available counting rates were plotted.)

On the NanoPET/CT, the total coincidence rate was constant at up to about 5 MBq of $^{99\text{m}}\text{Tc}$ and then increased to a maximum at 175 MBq (Fig. 3C).

The spatial resolution degraded when high $^{99\text{m}}\text{Tc}$ activity was present with the ^{22}Na point source (Figs. 4A–4C). The full width at half maximum was broadened by 20% at 1.8, 115, and 110 MBq of $^{99\text{m}}\text{Tc}$ for the Genisys4, Inveon, and NanoPET/CT, respectively.

Random Coincidences from $^{99\text{m}}\text{Tc}$ Background on NanoPET/CT

To verify that the increased counting rate on the NanoPET/CT in Study 2A was due to random coincidences, 500 MBq of $^{99\text{m}}\text{Tc}$ were imaged alone. The coincidence counting rate (plotted as randoms in Fig. 3C) followed the same trajectory as seen in Study 2A, though this time rising from a baseline of almost zero coincidences for activities below 5 MBq to a maximum for 175 MBq, approximately the same activity as in Study 2A. The calculated true coincidence counting rate is also plotted in Figure 3C.

Counting Rate Capability with ^{22}Na Source and ^{177}Lu Background

On the NanoPET/CT, use of the therapeutic radionuclide ^{177}Lu gave results similar to those found for $^{99\text{m}}\text{Tc}$. At ^{177}Lu activities higher than 10 MBq, the counting rate increased quickly (Fig. 3C). The maximum activity used, 88 MBq, did not clearly affect the spatial resolution (Fig. 4C). The main γ -emission for $^{99\text{m}}\text{Tc}$ at 140 keV has a photon yield of 89%, and the most prominent γ -emissions from ^{177}Lu at 113 and 208 keV have a photon yield of 6.4% and 11.0%, respectively. Assuming these all interact in the detectors with the same probability, we need roughly 5 times the activity of ^{177}Lu to have the same photon fluence rate as for $^{99\text{m}}\text{Tc}$.

Counting Rate Capability with ^{18}F Source and $^{99\text{m}}\text{Tc}$ Background

Comparisons of the counting rate with and without $^{99\text{m}}\text{Tc}$ are found in Figures 5A, 5B, and 5C for the Genisys4, Inveon, and NanoPET/CT, respectively. Introduction of $^{99\text{m}}\text{Tc}$ into the field of view resulted in divergence of coincidence counting rates from those found for ^{18}F alone. The initial activities of $^{99\text{m}}\text{Tc}$ disrupted the counting rate for all systems. As both the ^{18}F and the $^{99\text{m}}\text{Tc}$ decayed, the divergence decreased. The response of the Genisys4 and Inveon was similar to that in Study 2A, with coincidence counts being lost in relation to the amount of $^{99\text{m}}\text{Tc}$ activity. At higher activities of the two radionuclides,

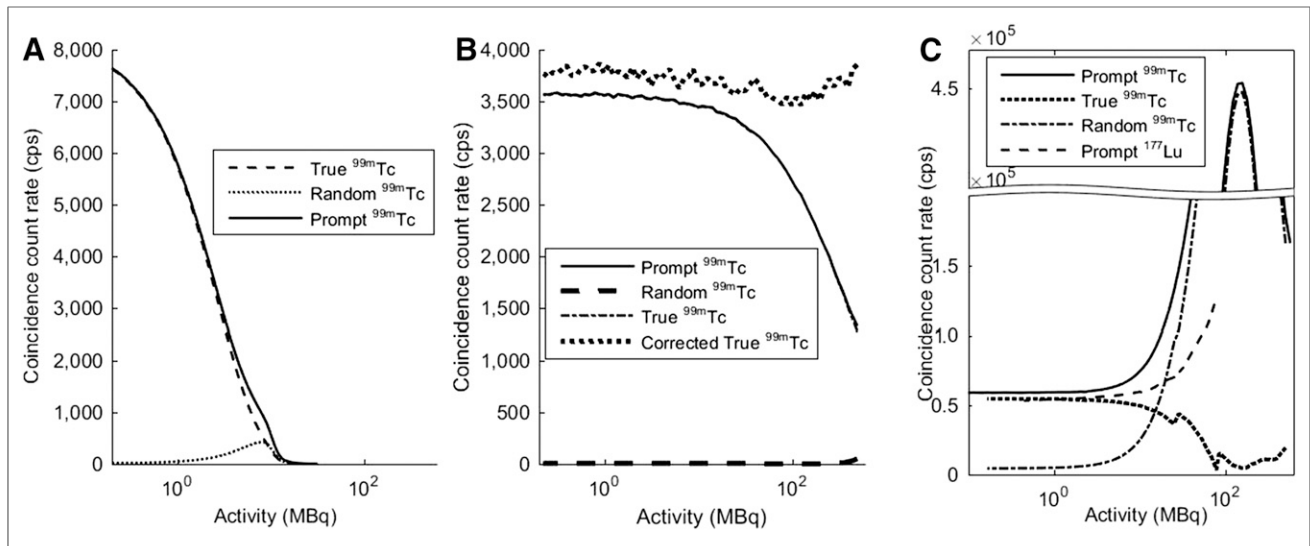


FIGURE 3. Coincidence counting rates when ^{22}Na point source was imaged together with decaying $^{99\text{m}}\text{Tc}$ (Study 2A) for Genisys4 (A), Inveon (B), and NanoPET/CT (C). B also presents corrected counting rate for Study 2A for Inveon. C also presents coincidence counting rates for decaying $^{99\text{m}}\text{Tc}$ (Study 2B) and ^{22}Na point source imaged together with decaying ^{177}Lu (Study 2C) on NanoPET/CT.

the NanoPET/CT experienced a higher counting rate loss because of dead time, but at lower activities the system measured a higher counting rate because of the high number of random counts.

The dead-time correction factor readily available to the user on the Inveon was able to correct the divergence, as seen in Figure 5B.

DISCUSSION

A leading strategy to find new and better treatments for cancer has been the development of targeted RPT that specifically finds and disseminates cancer cells. A ligand–radionuclide radiopharmaceutical can be applied either as a primary therapy or,

through a dual or even synergetic effect, as a way to activate the body’s own immune system and inhibit the signaling vital to the cancer cell. For aggressive cancers with a poor prognosis that have been difficult to treat thus far, regimens consisting of various combination of targeted treatments might be a future strategy. To optimize such strategies, it will be crucial to accurately quantify the response in vivo during and after therapy. Changes in tumor size, tumor viscosity, the extracellular microenvironment, and other factors that enable and limit the tumor can be prognostic and can help inform decisions on further treatment. A comprehensive review has been published previously by Vallabhajosula (17).

This study has shown the feasibility of performing intratherapeutic imaging on preclinical PET systems. The intricate data

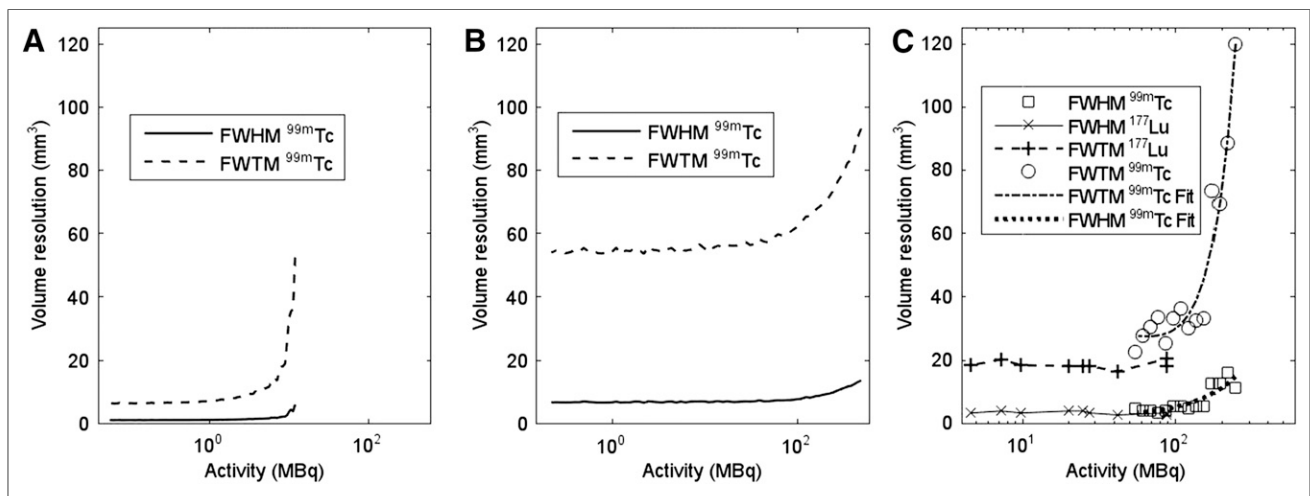


FIGURE 4. Volume resolution for Genisys4 (A), Inveon (B), and NanoPET/CT (C) measured over ^{22}Na point source imaged together with decaying $^{99\text{m}}\text{Tc}$ (Study 2A). C also presents volume resolution measured over ^{22}Na point source together with decaying ^{177}Lu for NanoPET/CT (Study 2C). FWHM = full width at half maximum; FWTM = full width at tenth maximum.

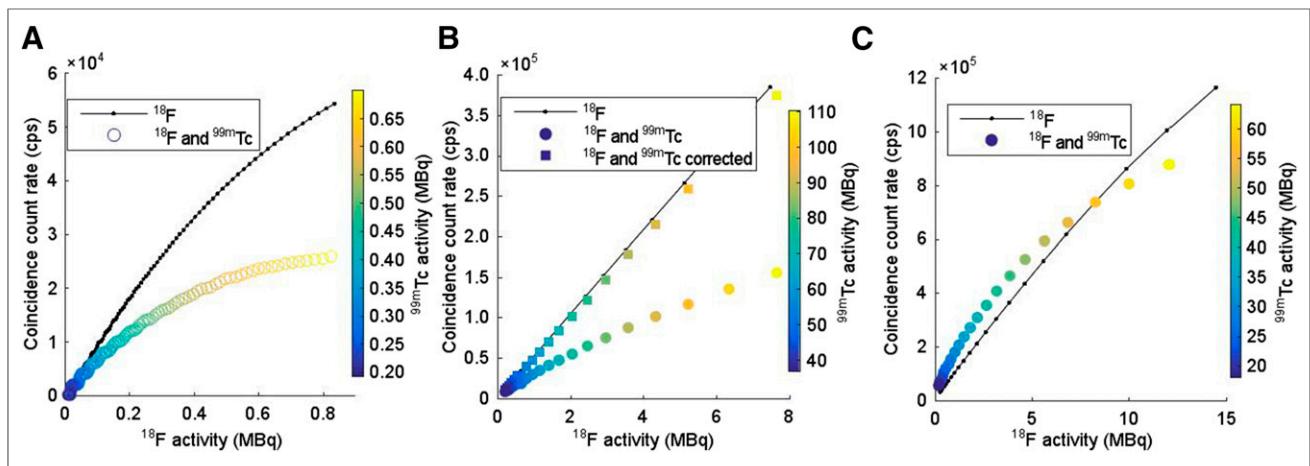


FIGURE 5. Comparison of true coincidence counting rates detected for ^{18}F decaying alone (Study 1) or together with $^{99\text{m}}\text{Tc}$ (Study 3) on Genisys4 (A), Inveon (B), and NanoPET/CT (C). (On NanoPET/CT, available counting rates were plotted.) B also presents corrected counting rate for Study 3 for Inveon.

processing in the investigated systems can, to a varying degree, handle a higher photon fluence impinging on the detector and creating high counting rates. In the case of the NanoPET/CT, even ^{177}Lu activities higher than those usually used in preclinical studies did not seem to diminish the spatial resolution. As shown in Figure 4C, $^{99\text{m}}\text{Tc}$ was a good surrogate for ^{177}Lu as measured on the NanoPET/CT (no such study was possible at UCLA because it lacks a ^{177}Lu license).

Because of the availability of $^{99\text{m}}\text{Tc}$ at nuclear medicine clinics and its comparatively low price, its use as a surrogate for a hypothetical therapeutic radionuclide is a helpful way to evaluate the plausibility of performing intratherapeutic imaging on PET systems. The main photon emission of $^{99\text{m}}\text{Tc}$, 140 keV, is comparable to the 113- and 208-keV photon emissions of ^{177}Lu . Since these photon emissions are likely to have approximately an equal probability of interacting in the detector and an equal effect on counting rate, equal photon fluences should result in similar counting rates and effects on the resolution. The difference in photon yield can therefore be used to approximate the activities of $^{99\text{m}}\text{Tc}$ and ^{177}Lu needed to result in comparable photon fluence rates.

The high sensitivity and lower counting rate capabilities of the Genisys4 reduce the amount of activity that can be handled by the system, including the PET radionuclide. The system loses a linear relationship between counting rate and activity at low activities, but this error might be compensated for fairly easily with an accurate dead-time correction model, as demonstrated on the Inveon (Fig. 2B). In the $^{99\text{m}}\text{Tc}$ activity interval investigated in Figure 3, the system never reached a constant counting rate. This is, however, expected to happen for low enough activities. The interval was chosen to imitate a photon fluence relevant in RPT. In the case of ^{177}Lu therapy, activities of 20–40 MBq are administered preclinically and would probably influence the performance of the Genisys4 since the detector system is paralyzed at 10 MBq of $^{99\text{m}}\text{Tc}$.

The Inveon and NanoPET/CT can handle the activity levels relevant to preclinical intratherapeutic imaging. Although the Genisys4 is limited by its dead-time losses, the Inveon and NanoPET/CT may suffer more from resolution losses due to event pile-up, as this increases with counting rate.

The spatial resolution was maintained on two of the systems up to therapeutic activities. Thus, for good image quality at high photon fluences, it is important to know the limitations of the system.

The NanoPET/CT showed an interesting higher tendency to produce random events from the $^{99\text{m}}\text{Tc}$, as the random coincidence rate started to increase when the $^{99\text{m}}\text{Tc}$ activity was higher than 5 MBq, leading to a net increase in the prompt coincidence counting rate for activities of up to 175 MBq. After a maximum counting rate had been reached, the effects of dead time dominated and the counting rate dropped.

CONCLUSION

We have presented a simple method of evaluating the counting rate capabilities of preclinical PET systems being used for intratherapeutic imaging. The evaluated systems showed a clear dependence on the higher impinging photon fluence rate, which affected both count losses and spatial resolution. For therapeutic ^{177}Lu activities of 10–50 MBq, two of the systems will start to experience a coincidence count loss, although with negligible loss of spatial resolution. The third investigated system was not able to handle such high activities.

DISCLOSURE

The costs of publication of this article were defrayed in part by the payment of page charges. Therefore, and solely to indicate this fact, this article is hereby marked “advertisement” in accordance with 18 USC section 1734. This research was supported by grants from the Swedish Cancer Society, Mrs. Berta Kamprad’s Foundation, Gunnar Nilsson’s Foundation, and Governmental Funding of Clinical Research within the National Health Service. No other potential conflict of interest relevant to this article was reported.

REFERENCES

1. Kramer-Marek G, Capala J. The role of nuclear medicine in modern therapy of cancer. *Tumour Biol.* 2012;33:629–640.
2. Mayson SE, Yoo DC, Gopalakrishnan G. The evolving use of radioiodine therapy in differentiated thyroid cancer. *Oncology.* 2015;88:247–256.

3. Goldsmith SJ. Radioimmunotherapy of lymphoma: Bexxar and Zevalin. *Semin Nucl Med.* 2010;40:122–135.
4. Druce MR, Lewington V, Grossman AB. Targeted radionuclide therapy for neuroendocrine tumours: principles and application. *Neuroendocrinology.* 2010;91:1–15.
5. Gulenchyn KY, Yao X, Asa SL, Singh S, Law C. Radionuclide therapy in neuroendocrine tumours: a systematic review. *Clin Oncol (R Coll Radiol).* 2012;24:294–308.
6. Larson SM, Carrasquillo JA, Cheung NK, Press OW. Radioimmunotherapy of human tumours. *Nat Rev Cancer.* 2015;15:347–360.
7. Fani M, Maecke HR. Radiopharmaceutical development of radiolabelled peptides. *Eur J Nucl Med Mol Imaging.* 2012;39(suppl 1):S11–S30.
8. Orlova A, Feldwisch J, Abrahamsén L, Tolmachev V. Update: Affibody molecules for molecular imaging and therapy for cancer. *Cancer Biother Radiopharm.* 2007;22:573–584.
9. Rajendran JG, Krohn KA. F-18 fluoromisonidazole for imaging tumor hypoxia: imaging the microenvironment for personalized cancer therapy. *Semin Nucl Med.* 2015;45:151–162.
10. Oxboel J, Brandt-Larsen M, Schjoeth-Eskesen C, et al. Comparison of two new angiogenesis PET tracers ⁶⁸Ga-NODAGA-E[c(RGDyK)]₂ and ⁶⁴Cu-NODAGA-E[c(RGDyK)]₂; in vivo imaging studies in human xenograft tumors. *Nucl Med Biol.* 2014;41:259–267.
11. Nguyen QD, Aboagye EO. Imaging the life and death of tumors in living subjects: preclinical PET imaging of proliferation and apoptosis. *Integr Biol (Camb).* 2010;2:483–495.
12. Germano G, Hoffman E. A study of data loss and mispositioning due to pileup in 2-D detectors in PET. *IEEE Trans Nucl Sci.* 1990;37:671–675.
13. Szanda I, Mackewn J, Patay G, et al. National Electrical Manufacturers Association NU-4 performance evaluation of the PET component of the NanoPET/CT preclinical PET/CT scanner. *J Nucl Med.* 2011;52:1741–1747.
14. Bai B, Dahlbom M, Park R, et al. Performance comparison of GENISYS4 and microPET preclinical PET scanners. In: *2012 IEEE Nuclear Science Symposium and Medical Imaging Conference Record (NSS/MIC)*. Piscataway, NJ, IEEE; 2012:3765–3768.
15. Bao Q, Newport D, Chen M, Stout DB, Chatziioannou AF. Performance evaluation of the Inveon dedicated PET preclinical tomograph based on the NEMA NU-4 standards. *J Nucl Med.* 2009;50:401–408.
16. Goertzen AL, Bao Q, Bergeron M, et al. NEMA NU 4-2008 comparison of preclinical PET imaging systems. *J Nucl Med.* 2012;53:1300–1309.
17. Vallabhajosula S. *Molecular Imaging: Radiopharmaceuticals for PET and SPECT*. New York, NY: Springer; 2009:215–254.